

Kitaev materials beyond iridates: order by quantum disorder and Weyl magnons in rare-earth double perovskites

Fei-Ye Li^{1,*}, Yao-Dong Li^{2,*}, Yue Yu^{2,4}, Arun Paramakanti³, and Gang Chen^{2,4,5†}

¹CAS Key Laboratory of Theoretical Physics, Institute of Theoretical Physics,
Chinese Academy of Sciences, Beijing 100190, People's Republic of China

²State Key Laboratory of Surface Physics, Center for Field Theory and Particle Physics,
Department of Physics, Fudan University, Shanghai 200433, People's Republic of China

³Department of Physics, University of Toronto, Toronto, Ontario,

Canada M5S 1A7 and Canadian Institute for Advanced Research, Toronto, Ontario, Canada M5G 1Z8

⁴Collaborative Innovation Center of Advanced Microstructures,
Nanjing, 210093, People's Republic of China and

⁵Perimeter Institute for Theoretical Physics, Waterloo, Ontario N2L 2Y5, Canada

(Dated: February 20, 2017)

Motivated by the experiments on the rare-earth double perovskites, we propose a generalized Kitaev-Heisenberg model to describe the generic interaction between the spin-orbit-entangled Kramers doublets of this new model. In the phase diagram, there exist large regions with a continuous $U(1)$ or $O(3)$ degeneracy. Since no symmetry of the model protects such a continuous degeneracy, we predict that the quantum fluctuation lifts the continuous degeneracy and favors various magnetic orders in the phase diagram. From this order by quantum disorder mechanism, we further predict that the magnetic excitations of the resulting ordered phases are characterized by nearly gapless pseudo-Goldstone modes. We find that there exist Weyl magnon excitations for certain magnetic orders. We expect our prediction to inspire further study of Kitaev physics, the order by quantum disorder phenomenon and topological spin wave modes in the rare-earth magnets and the systems alike.

I. INTRODUCTION

There has been an intensive interest in the study of Kitaev materials^{1–15}. Originally, Kitaev materials refer to honeycomb^{1,2,16,17}, hyperhoneycomb^{9,18,19}, harmonic honeycomb¹¹, and hyperkagome iridates^{20–22}, and more recently, have been extended to the new material RuCl_3 ^{23–25}. In these systems, the magnetic ions are heavy elements like Ir^{4+} and Ru^{4+} , where the spin-orbit coupling (SOC) is quite strong. Due to the spin-orbit entanglement of the local moments, the interaction between them depends on the bond orientation^{1,21,26,27}, and may involve a large Kitaev spin interaction¹. Since Kitaev model²⁸ supports a robust quantum spin liquid ground state, one goal of exploring these systems is to realize the Kitaev spin liquid with a dominant Kitaev interaction. More generally, it is of great importance to understand the role of spin-orbit entanglement on the properties of a strongly correlated quantum many-body system²⁹.

Since the Kitaev interaction¹, or more precisely, the bond dependent spin interaction, is a natural consequence of the strong SOC²¹, its presence should go beyond iridates or ruthenates. The vast families of rare-earth magnets have *never* been explored along the line of Kitaev interaction. In fact, rare-earth moments have much stronger SOC than iridium or ruthenium^{30–38}. The $4f$ electrons are much more localized than the $5d$ or $4d$ electrons in iridates and ruthenates. Most often, the interaction between the local moments in the rare earth systems is merely restricted to the nearest neighbors, while the iridates or ruthenates may involve significant

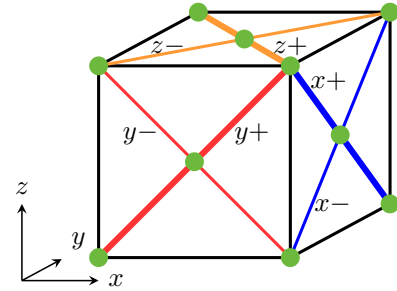


FIG. 1. (Color online.) The bond dependent interactions in the FCC lattice. We have marked the six distinct bond types γ_{\pm} ($\gamma = x, y, z$), that have the specific forms of bond-dependent interactions in Eq. 1. The inset is the global coordinate system that defines the spin components.

further neighbor interactions due to the extended electron wavefunctions³⁹. Moreover, the rare-earth elements do not suffer from the neutron absorption issue that prevails in the study of iridates^{16,17}. Because of the small energy scale of the interaction, the external magnetic field and the inelastic neutron scattering could even be used to precisely determine the Hamiltonian of the rare-earth systems. All these advantages make the rare-earth systems ideal Kitaev materials.

In this paper, we turn from iridates to the rare-earth systems and explore the consequence of the spin-orbit entanglement and the Kitaev interaction in rare-earth double perovskites. Double perovskite ($\text{A}_2\text{BB}'\text{O}_6$) is a very common system in which the magnetic ions B' form

a face-centered-cubic (FCC) lattice^{26,27,40}. Previously, the interplay of strong correlation and strong SOC has been explored for the $4d$ and $5d$ transition metal elements with partially filled t_{2g} shells^{26,27}. It was pointed out that the strong spin-orbit entanglement gives a multipolar structure of the local moments and rich magnetic multipolar orders^{26,27}. In contrast, the rare-earth electrons often experience substantial crystal electric field (CEF) that splits the $(2J+1)$ -fold degeneracy of the spin-orbit-entangled total moment \mathbf{J} . For a half-integer moment J , the CEF ground state is a Kramers' doublet whose degeneracy is protected by the time reversal symmetry. Often, the CEF gap is much larger than the temperature scale and exchange interaction in the system, and the low-temperature magnetic properties are fully captured by the ground state doublets that are modeled by pseudospin-1/2 local moments.

For the rare-earth double perovskites ($\text{Ba}_2\text{LnSbO}_6$, Ln = rare earths)⁴⁰⁻⁴⁵, we propose a generic model on the FCC lattice that describes the nearest-neighbor interaction between the Kramers' doublet local moments. This generic model involves the Heisenberg interaction, the Kitaev interaction, and an additional crossing exchange that is symmetric in two pseudospin components. In the mean-field phase diagram of this generic model, we find large parameter regions that support ground states with continuous degeneracies. Due to the spin-orbit entanglement, the generic model does not have any continuous symmetry. The continuous degeneracy is thus accidental and not related to any microscopic symmetry of the model. We expect that, the quantum fluctuations should break the accidental degeneracy and favor magnetic ordered states. This mechanism is known as order by quantum disorder (ObQD)^{36,46-48}. Because of the continuous degeneracy, the fluctuations within the degenerate mean-field ground state manifold are very soft. Quantum fluctuations in a systematic $1/S$ expansion would lead to a small gap and a pseudo-Goldstone mode for large S , leading to a regime of temperatures with an additional magnetic contribution to the specific heat, $C_{\text{mag}} \sim T^3$. The impact of large quantum fluctuations for $S = 1/2$ may further enhance the ObD gap; there is no controlled theory in this regime. In addition to the pseudo-Goldstone mode, the Weyl magnon mode⁴⁹ is found in the magnetic excitation for certain magnetic order. In contrast to the low energy pseudo-Goldstone mode, the Weyl magnon mode appears at finite energies due to the bosonic nature of the spin wave excitation.

This paper is organized as follows. In Sec. II, we derive the generalized Kitaev-Heisenberg model. We present a systematic analysis of the mean-field phase diagram of this model in Sec. III. Competition between different interactions, together with the geometrical frustration, leads to a very rich phase diagram. Specifically, among different phases, we focus on the regions with a continuous $U(1)$ or $O(3)$ degeneracy, in Sec. IV. The degeneracy at the mean-field level is lifted when the quantum fluctuation is included, and various magnetic orders are

favored in these regions. We demonstrate the ObQD explicitly. We further show the magnetic excitations of the resultant ordered phases are characterized by the pseudo-Goldstone mode with a nearly gapless dispersion. Finally, we conclude with a discussion in Sec. V.

II. THE GENERALIZED KITAEV-HEISENBERG MODEL

We focus on a series of double perovskite-type oxides⁴⁰, $\text{Ba}_2\text{LnSbO}_6$ (Ln = rare earth), where the Ba ions are located at the A sites of the perovskite-type oxides ABO_3 , and the Ln and Sb ions are regularly ordered at the B sites. Specifically, the Ln and Sb ions are ordered in the rock-salt type structure, with space group $\text{Fm}\bar{3}\text{m}$. Each of the two kinds of ions forms a separate FCC lattice. The magnetic behavior depends on the Ln^{3+} ions ($[\text{Xe}]4f^n$, $[\text{Xe}]$: electronic xenon core), where the SOCs are typically quite large. We study the Kramers' doublet that is formed by the $4f$ electrons of the Ln^{3+} ion with an odd n when the crystal electric field enters.

Under the $\text{Fm}\bar{3}\text{m}$ space group symmetry, the pseudospin, \mathbf{S} , that acts on the Kramers' doublet of the rare earth ion, transforms as a pseudovector. Both the pseudospin position and the pseudospin orientation are transformed. The most general exchange interaction between the local moments on the nearest neighbor sites, allowed by the lattice symmetry, is a generalized Kitaev-Heisenberg model with

$$H = \sum_{\langle ij \rangle_{\gamma\pm}} [J \mathbf{S}_i \cdot \mathbf{S}_j + K S_i^\gamma S_j^\gamma \pm F(S_i^\alpha S_j^\beta + S_i^\beta S_j^\alpha)], \quad (1)$$

where the bond index $\gamma\pm$ refers to the specific interaction that depends on the orientation of the bond in the plane and the pseudospin components are defined in the global coordinate system (see Fig. 1). We expect the nearest neighbor interaction is sufficient to describe the magnetic properties of the rare-earth moments in this system as the $4f$ electrons are very localized spatially. Besides the ordinary isotropic Heisenberg exchange interaction, we have the well-known Kitaev exchange interaction as well as the symmetric pseudo-dipole interaction that depends on the bond orientation. In Eq. 1, the antisymmetric Dzyaloshinskii-Moriya interaction is prohibited by the inversion symmetry of the system⁵⁰. The component γ ($= x, y, z$) specifies the three distinct types of Ising coupling in the Kitaev exchange (K term), and $\{\alpha, \beta, \gamma\}$ is a cyclic permutation of $\{x, y, z\}$, that contributes to the symmetric pseudo-dipole interaction (F term). The bond dependent pseudospin interaction is a direct consequence of the spin-orbit entanglement and widely occurs in many strong spin-orbit-coupled materials^{1,21,26,27,38}.

This generalized Kitaev-Heisenberg model was obtained previously by one of the authors and his collaborators in the context of the iridium-based double perovskites La_2BIrO_6 ($\text{B} = \text{Mg, Zn}$)^{51,52}. In the previous

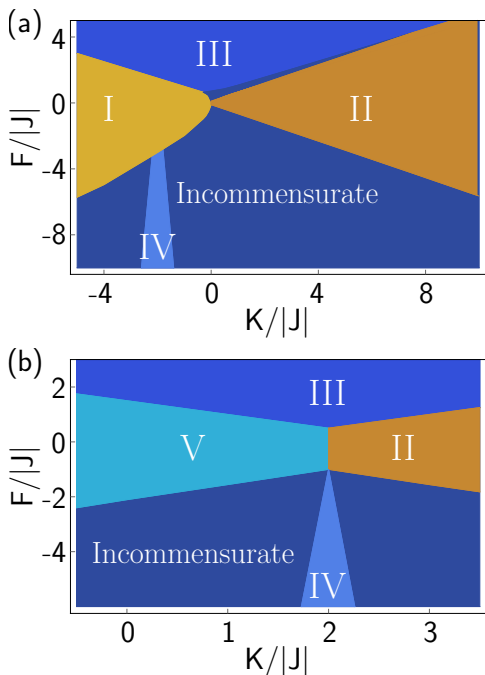


FIG. 2. (Color online.) The mean-field phase diagrams for an antiferromagnetic Heisenberg coupling (a) and for a ferromagnetic Heisenberg coupling (b). The incommensurate phase has non-uniform spin amplitudes on every site. Both phase I and phase II have antiferromagnetic collinear orders with the wavevector X , and a continuous $U(1)$ ground state degeneracy exists in phase II. Both phase III and phase IV have antiferromagnetic collinear orders with the wavevector L , and phase IV shows a $U(1)$ degeneracy. Phase V is ferromagnetically ordered with an $O(3)$ ground state degeneracy. See the main text and Tab. I for a detailed discussion. The lattice constant of the FCC lattice is set to unity throughout the paper.

works, the mean-field phase diagram in the antiferromagnetic Heisenberg regime was obtained with classical mean-field theory and classical Monte Carlo⁵¹, and the spin-wave spectrum was compared to the experiments in the regime with a dominant Kitaev interaction and a sizeable second-neighbor ferromagnetic interactions between the iridium local moments⁵². Here, our motivation and purpose in this paper is different. We are inspired by the magnetic properties of the rare-earth double perovskites that host $4f$ electrons. As we have explained in Sec. I, the exchange interaction of $4f$ local moments is short-ranged and we only keep the nearest-neighbor interactions. This clearly differs from iridates. For iridates, there are five electrons (or one hole) in the triply degenerate t_{2g} orbitals for the magnetic ion Ir^{4+} in the cubic crystal field environment. The atomic spin-orbit coupling is active on the t_{2g} orbitals and entangles the atomic spin with the orbitals. The simplicity of the spin-orbit-entangled wavefunction and the Ir-O-Ir exchange path allows the determination of the exchange interaction from a microscopic perspective^{13,21}. The Heisenberg part of the ex-

Phase	Wavevector	Order Para.	Continuous deg
I	$(2\pi, 0, 0)$	along $[100]$ axis	–
II	$(2\pi, 0, 0)$	in (100) plane	$U(1)$
III	(π, π, π)	along $[111]$ axis	–
IV	(π, π, π)	in (111) plane	$U(1)$
V	$(0, 0, 0)$	any direction	$O(3)$

TABLE I. The mean-field phases in Fig. 2. The incommensurate phase is not included here.

change interaction for iridates is often antiferromagnetic, and that is the reason that the previous work on the iridate double perovskites⁵¹ studied this regime. Because of the spatial extension of the Ir 5d electrons, the previous work on iridates further explored the second neighbor exchange interaction⁵². In contrast, the wavefunction of the Kramers doublet for the rare-earth moments arises from the combined effect of the atomic spin-orbit coupling and the crystal electric field and depends sensitively on the crystal electric field Hamiltonian that acts on the spin-orbit-entangled total moments. As a result, the exchange interaction between the rare-earth local moments varies for different wavefunctions of the Kramers doublets. Moreover, from the experience on rare-earth pyrochlore materials, many different parameter regimes can occur^{36,53}. So we explore all parameter range for the rare-earth double perovskites. In particular, while previous work on the iridates^{51,52} only studied the case of antiferromagnetic first neighbor coupling $J > 0$, here we also allow a ferromagnetic $J < 0$. In the remaining sections, we study this generalized Kitaev-Heisenberg model in all parameter regimes and obtain the magnetic properties and the magnetic excitations.

Compared with the rare-earth triangular system^{37,38,54} and the pyrochlore system^{30,32,34}, there are only three independent pseudospin interactions in Eq. 1. It is the symmetries of the FCC lattice that help reduce the number of independent pseudospin interactions in our model. This result indicates that one may find even simpler models in strong spin-orbit-coupled systems with large lattice symmetries.

III. MEAN-FIELD PHASE DIAGRAM

We now discuss the mean-field phase diagram of the generalized Kitaev-Heisenberg model in Eq. 1. We systematically analyze the mean-field ground states in different parameter regimes. We consider both antiferromagnetic and ferromagnetic Heisenberg interactions with $J > 0$ and $J < 0$, respectively.

In the classical mean-field theory, we first treat the pseudospin as a classical vector that satisfies the hard constraint $|\mathbf{S}_i| = S$. The classical (mean-field) energy of the system needs to be optimized under this local constraint on every lattice site. This procedure is difficult as the local hard constraint is hard to implement. Instead,

we here adopt the well-known Luttinger-Tisza method⁵⁵ that is to replace the local hard spin constraint by a global one such that

$$\sum_i |\mathbf{S}_i|^2 = NS^2, \quad (2)$$

where N is the total number of the pseudospins in the system. We optimize the classical mean-field energy,

$$E_{\text{cl}} = \sum_{\mathbf{q}} \sum_{\alpha\beta} \mathcal{E}_{\alpha\beta}(\mathbf{q}) S_{\mathbf{q}}^{\alpha} S_{-\mathbf{q}}^{\beta}, \quad (3)$$

under the global constraint. Here we have defined

$$S_i^{\alpha} = \frac{1}{N^{\frac{1}{2}}} \sum_{\mathbf{q}} S_{\mathbf{q}}^{\alpha} e^{i\mathbf{q}\cdot\mathbf{r}_i}. \quad (4)$$

Once the mean-field ground state satisfies both the global constraint and the local hard spin constraint, then the ground state under this approximation turns out to be the real ground state of the model in the classical limit.

In Fig. 2, we depict the mean-field phase diagram with both antiferromagnetic and ferromagnetic Heisenberg interactions. The antiferromagnetic case with $J > 0$ has a large classical degeneracy of ordered states, so that even a small Kitaev and F coupling can influence the nature of the ground state in the vicinity of the pure Heisenberg point. However, for the ferromagnetic case with $J < 0$, the anisotropic couplings primarily lead to pinning of the moments for small strengths, but large anisotropic couplings can change the nature of the ordered state. In the phase diagram, there is a large region where the minimum of the mean-field energy occurs in a set of incommensurate wavevectors (see Fig. 2). In these incommensurate regions, only one spin component is involved in the mean-field ground state. As a result, this incommensurate state cannot satisfy the local hard spin constraint due to the incommensurability. This result indicates the strong frustration in these regions of the generalized Kitaev-Heisenberg model. It is noted that the mean-field phase diagram in the regime with $-2 < F/J < 2$, $-2 < K/J < 2$ and $J > 0$ is obtained in the previous work⁵¹.

We continue with other ordered phases in the phase diagram. In Fig. 2a, phase I is an antiferromagnetic state with the ordering wavevector at $\mathbf{X} = (2\pi, 0, 0)$ or equivalently $(0, 2\pi, 0)$, $(0, 0, 2\pi)$. In this state, the spins order in a collinear pattern. For the $(2\pi, 0, 0)$ ordering wavevector, the spin ordering is locked to the \hat{x} direction with,

$$\text{I: } \mathbf{S}_i \equiv S \hat{m}_i = S \hat{x} e^{2\pi x_i}, \quad (5)$$

where x_i is the x coordinate of the lattice site \mathbf{r}_i . The locking between the ordering wavevector and the spin orientation is a direct consequence and general phenomenon of the strong spin-orbit-coupled magnets.

In phase II with a dominant and antiferromagnetic Kitaev interaction ($K > 0$), the system also orders with

the wavevector \mathbf{X} and equivalent ones. Although having the same ordering wavevector, the ground state of phase II has a continuous $U(1)$ degeneracy. If we choose the $(2\pi, 0, 0)$ ordering wavevector, the ground state is parameterized as

$$\text{II: } \mathbf{S}_i \equiv S \hat{m}_i = S [\cos \theta \hat{y} + \sin \theta \hat{z}] e^{2\pi x_i}, \quad (6)$$

where θ is an angular variable. This $U(1)$ degeneracy can be well understood, because the classical energy gained from the antiferromagnetic K term remains invariant when spin vectors are rotated within the $U(1)$ manifold. Here the presence of a weak pseudo-dipole interaction does not lift the degeneracy. At the mean field level, phase I and phase II are understood as the easy axis along the $[100]$ direction and easy plane anisotropy in the (100) plane for the order parameter, respectively. Note that in region II there also exists a line degeneracy from \mathbf{X} to \mathbf{W} in the reciprocal space. Since only one spin component is involved, therefore, however, it can not form a normalized spin spiral order.

In the regimes dominated by the pseudo-dipole interaction (F term), we obtain two other ordered phases. Phase III is an antiferromagnetic ordered phase with the ordering wavevector $\mathbf{L} = (\pi, \pi, \pi)$ or equivalent ones. Given $\mathbf{L} = (\pi, \pi, \pi)$, the spin ordering is locked to the $[111]$ direction with

$$\text{III: } \mathbf{S}_i \equiv S \hat{m}_i = \frac{S}{\sqrt{3}} (\hat{x} + \hat{y} + \hat{z}) e^{i\pi(x_i + y_i + z_i)}. \quad (7)$$

Finally, phase IV has the same ordering wavevector as phase III but has a $U(1)$ ground state degeneracy. For the (π, π, π) ordering, the spin vector is parameterized as

$$\text{IV: } \mathbf{S}_i \equiv S \hat{m}_i = S (\cos \theta \hat{u}_1 + \sin \theta \hat{u}_2) e^{i\pi(x_i + y_i + z_i)}, \quad (8)$$

where θ is an angular variable, and \hat{u}_1, \hat{u}_2 are two unit vectors in the (111) plane, chosen as $\hat{u}_1 = [1\bar{1}0]/\sqrt{2}$, $\hat{u}_2 = [11\bar{2}]/\sqrt{6}$. At the mean field level, phase III and Phase IV can be understood as the easy axis along the $[111]$ direction and easy plane anisotropy in the (111) plane of the order parameter, respectively. Furthermore, like the case in phase II, a line degeneracy exists in the reciprocal space, from \mathbf{L} to another equivalent \mathbf{L} (e.g. from (π, π, π) to $(\pi, \pi, -\pi)$). Since the spins do not have uniform magnitudes, they cannot be the ground states.

When the Kitaev interaction is switched to ferromagnetic with $K < 0$ and remains dominant, the ground state depends on the sign of the Heisenberg interaction. The case with an antiferromagnetic Heisenberg interaction gives phase I. For the ferromagnetic Heisenberg interaction with $J < 0$, however, the classical ground state is a simple ferromagnetic state (phase V) but has an $O(3)$ degeneracy. The spin order is parametrized by two angular variables,

$$\text{V: } \mathbf{S}_i \equiv S \hat{m}_i = S (\sin \theta \cos \phi \hat{x} + \sin \theta \sin \phi \hat{y} + \cos \theta \hat{z}), \quad (9)$$

where θ runs from 0 to π , and ϕ runs from 0 to 2π . The $O(3)$ degeneracy, as in the previous $U(1)$ degeneracy case,

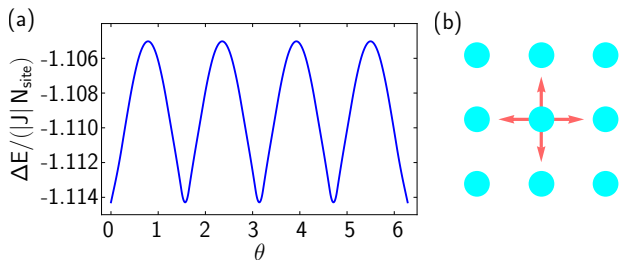


FIG. 3. (Color online.) Quantum zero point energy in $X = (2\pi, 0, 0)$ ordered state (phase II). (a) The minimum of ΔE occurs at $\theta = n\pi/2$ with $n \in \mathbb{Z}$. (b) Arrows indicate four-fold symmetry equivalent pseudospin orientation in the (100) plane. We choose $(J, K, F) = (1, 1, 0)$.

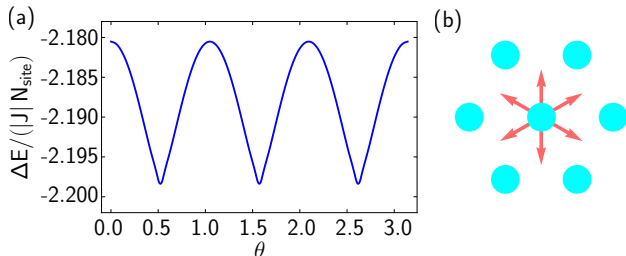


FIG. 4. (Color online.) Quantum zero point energy in $L = (\pi, \pi, \pi)$ ordered state (phase IV). (a) The minimum of ΔE occurs at $\theta = \pi/6 + n\pi/3$ with $n \in \mathbb{Z}$. (b) Arrows indicate six-fold symmetry equivalent pseudospin orientation in the (111) plane. We choose $(J, K, F) = (-1, 2, -4)$.

is understood from the invariance of the dominant classical energy from the ferromagnetic Kitaev interaction.

As we summarize in Tab. I, these five ordered phases have rather different order parameters. The phase transition between them, if there exists a direct transition between them, is first order.

IV. QUANTUM FLUCTUATION AND MAGNETIC EXCITATION

We focus on the ordered phases with a continuous ground state degeneracy, and discuss the role of quantum fluctuation when the quantum nature of the pseudospin is considered. Since the microscopic Hamiltonian only has discrete lattice symmetries, the continuous degeneracy of the mean-field ground states is not granted at the quantum level. We, therefore, expect that the degeneracy in the mean-field level will be lifted when quantum fluctuation is included. Within the linear spin wave theory, we now discuss this order by quantum disorder (ObQD) effect explicitly.

For the ground state with a continuous $U(1)$ degeneracy, parametrized as in Eq. 6 and Eq. 8, we introduce the Holstein-Primakoff bosons to express the spin operators

as

$$\mathbf{S}_i \cdot \hat{m}_i = S - b_i^\dagger b_i, \quad (10)$$

$$\mathbf{S}_i \cdot \hat{n}_i = \frac{(2S)^{\frac{1}{2}}}{2} (b_i + b_i^\dagger), \quad (11)$$

$$\mathbf{S}_i \cdot (\hat{m}_i \times \hat{n}_i) = \frac{(2S)^{\frac{1}{2}}}{2i} (b_i - b_i^\dagger), \quad (12)$$

where \hat{m}_i is the unit vector describing the spin orientation of classical spin order at site i , \hat{n}_i is a unit vector normal to \hat{m}_i , and $S = 1/2$. We substitute the spin operators with these Holstein-Primakoff bosons. In the linear spin wave approximation, we keep the boson terms up to the quadratic order. The resulting linear spin wave Hamiltonian has the following form

$$H_{sw} = \sum_{\mathbf{k}} \left[\sum_{\mu, \nu} (A_{\mu\nu}(\mathbf{k}) b_{\mathbf{k}\mu}^\dagger b_{\mathbf{k}\nu} + B_{\mu\nu}(\mathbf{k}) b_{-\mathbf{k}, \mu} b_{\mathbf{k}\nu} + B_{\mu\nu}^*(-\mathbf{k}) b_{\mathbf{k}\mu}^\dagger b_{-\mathbf{k}, \nu}^\dagger) + C(\mathbf{k}) \right] + E_{cl}, \quad (13)$$

where E_{cl} is the classical mean-field energy of the ground state and independent of the angular variable θ due to the $U(1)$ degeneracy, $A_{\mu\nu}$, $B_{\mu\nu}$ and C depend on θ , and $A_{\mu\nu}$, $B_{\mu\nu}$ satisfy

$$A_{\mu\nu}(\mathbf{k}) = A_{\nu\mu}^*(\mathbf{k}), \quad (14)$$

$$B_{\mu\nu}(\mathbf{k}) = B_{\nu\mu}(-\mathbf{k}). \quad (15)$$

While the classical mean-field energy E_{cl} preserves the $U(1)$ degeneracy, the quantum fluctuation lifts this continuous degeneracy through the quantum zero point energy ΔE that is given by

$$\Delta E = \sum_{\mathbf{k}} \left[\sum_{\mu} \frac{1}{2} (\omega_{\mu}(\mathbf{k}) - A_{\mu\mu}(\mathbf{k})) + C(\mathbf{k}) \right], \quad (16)$$

where $\omega_{\mu}(\mathbf{k})$ is the excitation energy of the μ -th spin wave mode at momentum \mathbf{k} .

In phase II where there is a $U(1)$ degeneracy (see Eq. 6), the minima of zero point energy ΔE occurs at

$$\text{II: } \theta = \frac{n\pi}{2}, \quad (17)$$

where $n \in \mathbb{Z}$, and the favored magnetic order has a four-fold symmetry equivalent configuration that is shown in Fig. 3.

In phase IV where there is also $U(1)$ degeneracy (see Eq. 8), the minima of zero point energy ΔE occurs at

$$\text{IV: } \theta = \frac{\pi}{6} + \frac{n\pi}{3}, \quad (18)$$

where $n \in \mathbb{Z}$ and the favored magnetic order has a six-fold symmetry equivalent configuration that is shown in Fig. 4.

Now we turn to phase V of the mean-field phase diagram, the ferromagnetic ordered state with an $O(3)$ degeneracy. As we have parametrized with a vector on a unit sphere in Eq. 9, two angular variables (θ and ϕ) are

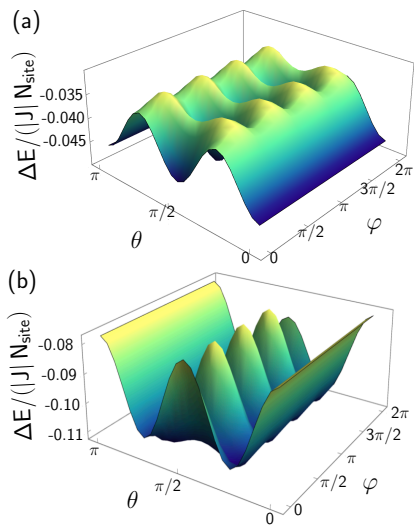


FIG. 5. (Color online.) Quantum zero point energy of two representative parameters in mean-field phase V. The two-dimensional sphere is parametrized by polar angle θ and azimuthal angle φ . (a) We set $(J, K, F) = (-1, 1, 0)$ for phase V_a in Fig. 6, the favored spin orientations are $\pm\hat{x}$, $\pm\hat{y}$, and $\pm\hat{z}$, corresponding to the six minima of ΔE . (b) We set $(J, K, F) = (-1, 0, 1)$ for phase V_b in Fig. 6, the favored spin orientations are [111] directions, corresponding to the eight minima of ΔE .

needed to capture the $O(3)$ degeneracy. The minima of the zero point energy ΔE are shown in Fig. 5. We find two distinct ordering patterns that are not equivalent under the lattice symmetry. As we depict in Fig. 6, the phase V of the mean-field phase diagram is split into two distinct phases (V_a and V_b). In V_a (V_b), the quantum fluctuation selects the [001] type ([111] type) of magnetic order.

The lifting of the $O(3)$ degeneracy is understood through a cubic anisotropy that is induced by the quantum fluctuation. The cubic anisotropy in the energy is given as

$$E_{\text{ani}} = \lambda_{\text{ani}}[(M^x)^4 + (M^y)^4 + (M^z)^4], \quad (19)$$

where \mathbf{M} is the order parameter of the ferromagnetic phase. In phase V_a , $\lambda_{\text{ani}} < 0$ and we have the [001] ordering. In phase V_b , $\lambda_{\text{ani}} > 0$ and we have the [111] ordering.

Having determined the ground state configurations, we further study the spin wave excitation spectra in different phases. The results are depicted along high symmetry momentum lines in Fig. 7. There are two qualitative features in the spin wave spectra. First, we observe gapless modes in Fig. 7 (a), (b) and (c). These pseudo-Goldstone modes are characteristic of the phase ordered due to quantum fluctuation that lifts the continuous degeneracy, in our case, phase II, IV and V. Although a gap is expected to be generated by anharmonic effects, nearly gapless dispersion is a possible experimental signature of the order by quantum disorder scenario. Sec-

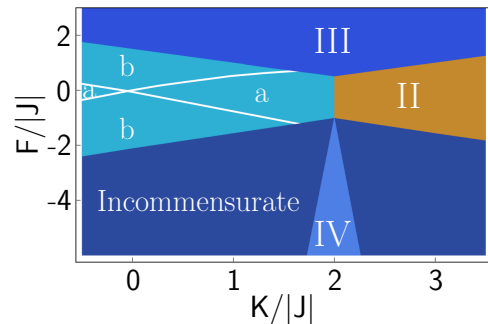


FIG. 6. (Color online.) Phase V in the mean-field phase diagram of Fig. 2 (b) is split into two phases with different magnetic orders once the quantum fluctuation is considered. Here $J < 0$.

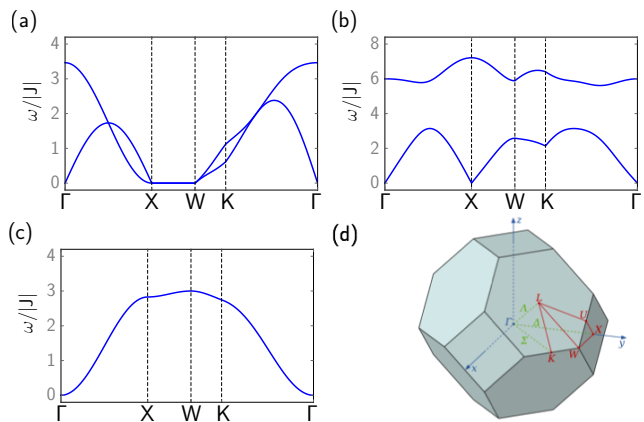


FIG. 7. (Color online.) The representative spin wave spectra along high symmetry momentum lines with (a) $(J, K, F) = (1, 1, 0)$ and $\theta = 0$ in phase II; (b) $(J, K, F) = (-1, 2, -4)$, $\theta = \pi/6$ in phase IV; (c) $(J, K, F) = (-1, 1, 0)$, $\theta = \pi/2$, $\varphi = 0$ in phase V_a . In (d) we depict the FCC Brillouin zone (the figure is adapted from Wikipedia⁵⁷).

ond, magnon spectrum in Fig. 7 (a) shows band touching (along $K-\Gamma$) due to accidental degeneracy, indicating the “Weyl magnon” behavior and the corresponding topologically robust surface states, although the Weyl node along $K-\Gamma$ belong to the type-II node⁵⁶ for the specific parameter choice in Fig. 7 (a). The Weyl band touching of the magnon spectrum is expected to be stable even beyond the linear spin-wave theory due to the robust topological nature.

V. DISCUSSION

Despite the abundance of the rare-earth double perovskites^{40,41}, the experimental characterization of them is quite limited. Only the crystal structure and the magnetic susceptibility measurements have been carried out so far. All these compounds are paramagnetic and have no magnetic ordering down to 1.8K⁴⁰. This result does

not mean all of them would be spin liquids. The temperature (1.8K) is not quite low for the rare-earth local moments since the exchange interaction between them is of the order of a couple Kelvin. It is very likely that the absence of magnetic ordering down to 1.8K is a thermal effect, and one could observe the ground state properties if the temperature is further lowered.

What would be the experimental phenomena that are expected for the ObQD phenomena and Weyl magnons? Clearly, one should observe one of the orders that we predict. Moreover, the consequence of the ObQD is the presence of the nearly gapless pseudo-Goldstone mode for the magnetic excitation. Strictly speaking, the pseudo-Goldstone mode should develop a minigap due to the anharmonic quantum effect, but one would expect a T^3 heat capacity in the temperature regime above the minigap energy scale. For the Weyl magnons, one could probe the spin wave spectrum with the inelastic neutron scattering measurement and directly detect the linear band touching. Alternatively, one could measure the consequence of Weyl magnons, such as the chiral surface state and optical conductivities. All these probes have been discussed in details in Ref. 49.

In many systems, the ObQD is very fragile because other small interactions, that are not included in the model, may simply drive the system into a different state. For rare-earth double perovskites, however, we expect the

dominant interaction is from the nearest neighbors. The further neighbor exchanges are rather weak due to the spatial localization of the $4f$ electrons. The remaining interaction is the magnetic dipole interaction that decays very fast with the separation of the local moments. The actual magnitude would depend on the material's details such as the the moment size and lattice constants. In any case, we expect the rare-earth double perovskites to be promising candidates for the ObQD phenomena.

The study of the rare-earth double perovskites is in the early stage. Many physical properties of the rare-earth double perovskites need to be measured, and it is very likely that other exotic quantum phases could emerge besides the ones that have been predicted here. We expect our work to bring further attention to this new class of materials.

Acknowledgements.—This work is supported by the Ministry of Science and Technology of People's Republic of China with the Grant No. 2016YFA0301001 (G.C.), NSERC of Canada (A.P.), the Start-Up Funds of Fudan University (Shanghai, People's Republic of China) and the Thousand-Youth-Talent Program (G.C.) of People's Republic of China. Research at Perimeter Institute is supported by the Government of Canada through the Department of Innovation, Science and Economic Development Canada and by the Province of Ontario through the Ministry of Research, Innovation and Science.

* These two authors contribute equally.

† gangchen.physics@gmail.com,
gchen_physics@fudan.edu.cn

¹ G. Jackeli and G. Khaliullin, "Mott Insulators in the Strong Spin-Orbit Coupling Limit: From Heisenberg to a Quantum Compass and Kitaev Models," *Phys. Rev. Lett.* **102**, 017205 (2009).

² J. Chaloupka, G. Jackeli, and G. Khaliullin, "Kitaev-Heisenberg Model on a Honeycomb Lattice: Possible Exotic Phases in Iridium Oxides $A_2\text{IrO}_3$," *Phys. Rev. Lett.* **105**, 027204 (2010).

³ H.-C. Jiang, Z.-G. Gu, X.-L. Qi, and S. Trebst, "Possible proximity of the mott insulating iridate Na_2IrO_3 to a topological phase: Phase diagram of the heisenberg-kitaev model in a magnetic field," *Phys. Rev. B* **83**, 245104 (2011).

⁴ J.-W. Mei, "Possible Fermi Liquid in the Lightly Doped Kitaev Spin Liquid," *Phys. Rev. Lett.* **108**, 227207 (2012).

⁵ I. I. Mazin, H. O. Jeschke, K. Foyevtsova, R. Valentí, and D. I. Khomskii, " Na_2IrO_3 as a molecular orbital crystal," *Phys. Rev. Lett.* **109**, 197201 (2012).

⁶ I. Kimchi and A. Vishwanath, "Kitaev-heisenberg models for iridates on the triangular, hyperkagome, kagome, fcc, and pyrochlore lattices," *Phys. Rev. B* **89**, 014414 (2014).

⁷ J. Chaloupka, G. Jackeli, and G. Khaliullin, "Zigzag Magnetic Order in the Iridium Oxide Na_2IrO_3 ," *Phys. Rev. Lett.* **110**, 097204 (2013).

⁸ M. Hermanns, K. O'Brien, and S. Trebst, "Weyl spin liquids," *Phys. Rev. Lett.* **114**, 157202 (2015).

⁹ T. Takayama, A. Kato, R. Dinnebier, J. Nuss, H. Kono,

L. S. I. Veiga, G. Fabbris, D. Haskel, and H. Takagi, "Hyperhoneycomb Iridate $\beta\text{-Li}_2\text{IrO}_3$ as a Platform for Kitaev Magnetism," *Phys. Rev. Lett.* **114**, 077202 (2015).

¹⁰ I. Rousochatzakis, J. Reuther, R. Thomale, S. Rachel, and N. B. Perkins, "Phase Diagram and Quantum Order by Disorder in the Kitaev $K_1 - K_2$ Honeycomb Magnet," *Phys. Rev. X* **5**, 041035 (2015).

¹¹ K. A. Modic, T. E. Smidt, I. Kimchi, N. P. Breznay, A. Biffin, S. Choi, R. D. Johnson, R. Coldea, P. Watkins-Curry, G. T. McCandless, J. Y. Chan, F. Gandara, Z. Islam, A. Vishwanath, A. Shekhter, R. D. McDonald, and J. G. Analytis, "Realization of a three-dimensional spinanisotropic harmonic honeycomb iridate," *Nat Commun* **5**, 4203 (2014).

¹² S. Nishimoto, V. M. Katukuri, V. Yushankhai, H. Stoll, U. K. Roszler, L. Hozoi, I. Rousochatzakis, and J. van den Brink, "Strongly frustrated triangular spin lattice emerging from triplet dimer formation in honeycomb Li_2IrO_3 ," *Nat Commun* **7**, 10273 (2016).

¹³ J. G. Rau, E. K.-H. Lee, and H.-Y. Kee, "Generic Spin Model for the Honeycomb Iridates beyond the Kitaev Limit," *Phys. Rev. Lett.* **112**, 077204 (2014).

¹⁴ J. Lou, L. Liang, Y. Yu, and Y. Chen, "Global phase diagram of the extended kitaev-heisenberg model on honeycomb lattice," arXiv preprint 1501.06990 (2015).

¹⁵ E. K.-H. Lee, J. G. Rau, and Y. B. Kim, "Two iridates, two models, and two approaches: A comparative study on magnetism in three-dimensional honeycomb materials," *Phys. Rev. B* **93**, 184420 (2016).

¹⁶ Y. Singh, S. Manni, J. Reuther, T. Berlijn, R. Thomale,

- W. Ku, S. Trebst, and P. Gegenwart, “Relevance of the heisenberg-kitaev model for the honeycomb lattice iridates $A_2\text{IrO}_3$,” *Phys. Rev. Lett.* **108**, 127203 (2012).
- 17 S. K. Choi, R. Coldea, A. N. Kolmogorov, T. Lancaster, I. I. Mazin, S. J. Blundell, P. G. Radaelli, Yogesh Singh, P. Gegenwart, K. R. Choi, S.-W. Cheong, P. J. Baker, C. Stock, and J. Taylor, “Spin waves and revised crystal structure of honeycomb iridate Na_2IrO_3 ,” *Phys. Rev. Lett.* **108**, 127204 (2012).
 - 18 S. Lee, E. K.-H. Lee, A. Paramekanti, and Y. B. Kim, “Order-by-disorder and magnetic field response in the heisenberg-kitaev model on a hyperhoneycomb lattice,” *Physical Review B* **89**, 014424 (2014).
 - 19 S. Lee, J.-S. Jeong, K. Hwang, and Y. B. Kim, “Emergent quantum phases in a frustrated J_1 - J_2 heisenberg model on the hyperhoneycomb lattice,” *Phys. Rev. B* **90**, 134425 (2014).
 - 20 Y. Okamoto, M. Nohara, H. Aruga-Katori, and H. Takagi, “Spin-Liquid State in the $S = 1/2$ Hyperkagome Antiferromagnet $\text{Na}_4\text{Ir}_3\text{O}_8$,” *Phys. Rev. Lett.* **99**, 137207 (2007).
 - 21 G. Chen and L. Balents, “Spin-orbit effects in $\text{Na}_4\text{Ir}_3\text{O}_8$: A hyper-kagome lattice antiferromagnet,” *Phys. Rev. B* **78**, 094403 (2008).
 - 22 G. Chen and Y. B. Kim, “Anomalous enhancement of the wilson ratio in a quantum spin liquid: The case of $\text{Na}_4\text{Ir}_3\text{O}_8$,” *Phys. Rev. B* **87**, 165120 (2013).
 - 23 J. A. Sears, M. Songvilay, K. W. Plumb, J. P. Clancy, Y. Qiu, Y. Zhao, D. Parshall, and Y.-J. Kim, “Magnetic order in α - RuCl_3 : A honeycomb-lattice quantum magnet with strong spin-orbit coupling,” *Phys. Rev. B* **91**, 144420 (2015).
 - 24 H.-S. Kim, Vijay Shankar V., Andrei Catuneanu, and H.-Y. Kee, “Kitaev magnetism in honeycomb RuCl_3 with intermediate spin-orbit coupling,” *Phys. Rev. B* **91**, 241110 (2015).
 - 25 A. Banerjee, C. A. Bridges, J. Q. Yan, A. A. Aczel, L. Li, M. B. Stone, G. E. Granroth, M. D. Lumsden, Y. Yiu, J. Knolle, S. Bhattacharjee, D. L. Kovrizhin, R. Moessner, D. A. Tennant, D. G. Mandrus, and S. E. Nagler, “Proximate kitaev quantum spin liquid behaviour in a honeycomb magnet,” *Nat Mater* **15**, 733–740 (2016).
 - 26 G. Chen, R. Pereira, and L. Balents, “Exotic phases induced by strong spin-orbit coupling in ordered double perovskites,” *Phys. Rev. B* **82**, 174440 (2010).
 - 27 G. Chen and L. Balents, “Spin-orbit coupling in d^2 ordered double perovskites,” *Phys. Rev. B* **84**, 094420 (2011).
 - 28 A. Kitaev, “Anyons in an exactly solved model and beyond,” *Annals of Physics* **321**, 2 – 111 (2006), january Special Issue.
 - 29 W. Witczak-Krempa, G. Chen, Y.B. Kim, and L. Balents, “Correlated quantum phenomena in the strong spin-orbit regime,” *Annual Review of Condensed Matter Physics* **5**, 57–82 (2014).
 - 30 S. H. Curnoe, “Structural distortion and the spin liquid state in $\text{Tb}_2\text{Ti}_2\text{O}_7$,” *Phys. Rev. B* **78**, 094418 (2008).
 - 31 J. S. Gardner, M. J. P. Gingras, and J. E. Greedan, “Magnetic pyrochlore oxides,” *Rev. Mod. Phys.* **82**, 53–107 (2010).
 - 32 S. Onoda and Y. Tanaka, “Quantum fluctuations in the effective pseudospin- $\frac{1}{2}$ model for magnetic pyrochlore oxides,” *Phys. Rev. B* **83**, 094411 (2011).
 - 33 S. Lee, S. Onoda, and L. Balents, “Generic quantum spin ice,” *Phys. Rev. B* **86**, 104412 (2012).
 - 34 Y.-P. Huang, G. Chen, and M. Hermele, “Quantum spin ices and topological phases from dipolar-octupolar doublets on the pyrochlore lattice,” *Phys. Rev. Lett.* **112**, 167203 (2014).
 - 35 Y.-D. Li and G. Chen, “Octupolar quantum spin ice: controlling spinons in a $U(1)$ quantum spin liquid,” arXiv preprint 1607.02287 (2016).
 - 36 L. Savary, K. A. Ross, B. D. Gaulin, J. P. C. Ruff, and L. Balents, “Order by quantum disorder in $\text{Er}_2\text{Ti}_2\text{O}_7$,” *Phys. Rev. Lett.* **109**, 167201 (2012).
 - 37 Y. Li, G. Chen, W. Tong, L. Pi, J. Liu, Z. Yang, X. Wang, and Q. Zhang, “Rare-earth triangular lattice spin liquid: A single-crystal study of YbMgGaO_4 ,” *Phys. Rev. Lett.* **115**, 167203 (2015).
 - 38 Y.-D. Li, X. Wang, and G. Chen, “Anisotropic spin model of strong spin-orbit-coupled triangular antiferromagnets,” *Phys. Rev. B* **94**, 035107 (2016).
 - 39 D. Pesin and L. Balents, “Mott physics and band topology in materials with strong spin-orbit interaction,” *Nature Physics* **6**, 376–381 (2010).
 - 40 S. Otsuka and Y. Hinatsu, “Structures and magnetic properties of rare earth double perovskites containing antimony or bismuth Ba_2LnMO_6 (Ln=rare earths; M=Sb, Bi),” *Journal of Solid State Chemistry* **227**, 132141 (2015).
 - 41 A. Dutta, P.K. Mukhopadhyay, T.P. Sinha, D. Das, and S. Shannigrahi, “Structural and magnetic properties of double perovskite oxide $\text{Ba}_2\text{CeSbO}_6$,” *Solid State Sciences* **58**, 64 – 69 (2016).
 - 42 T. Aharen, J. E. Greedan, C. A. Bridges, Adam A. Aczel, J. Rodriguez, G. MacDougall, G. M. Luke, T. Imai, V. K. Michaelis, S. Kroeker, H. Zhou, C. R. Wiebe, and L. M. D. Cranswick, “Magnetic properties of the geometrically frustrated $s = \frac{1}{2}$ antiferromagnets, $\text{La}_2\text{LiMoO}_6$ and Ba_2YMoO_6 , with the b-site ordered double perovskite structure: Evidence for a collective spin-singlet ground state,” *Phys. Rev. B* **81**, 224409 (2010).
 - 43 C. R. Wiebe, J. E. Greedan, P. P. Kyriakou, G. M. Luke, J. S. Gardner, A. Fukaya, I. M. Gat-Malureanu, P. L. Russo, A. T. Savici, and Y. J. Uemura, “Frustration-driven spin freezing in the $s = \frac{1}{2}$ fcc perovskite $\text{Sr}_2\text{MgReO}_6$,” *Phys. Rev. B* **68**, 134410 (2003).
 - 44 C. R. Wiebe, J. E. Greedan, G. M. Luke, and J. S. Gardner, “Spin-glass behavior in the $s = 1/2$ fcc ordered perovskite $\text{Sr}_2\text{CaReO}_6$,” *Phys. Rev. B* **65**, 144413 (2002).
 - 45 A. S. Erickson, S. Misra, G. J. Miller, R. R. Gupta, Z. Schlesinger, W. A. Harrison, J. M. Kim, and I. R. Fisher, “Ferromagnetism in the mott insulator $\text{Ba}_2\text{NaOsO}_6$,” *Phys. Rev. Lett.* **99**, 016404 (2007).
 - 46 C. L. Henley, “Ordering by disorder: Groundstate selection in fcc vector antiferromagnets,” *Journal of Applied Physics* **61**, 3962–3964 (1987).
 - 47 J. Villain, R. Bidaux, J.P. Carton, and R. Conte, “Order as an effect of disorder,” *J. Phys. (Paris)* **41**, 1263 (1980).
 - 48 M. E. Zhitomirsky, M. V. Gvozdikova, P. C. W. Holdsworth, and R. Moessner, “Quantum order by disorder and accidental soft mode in $\text{Er}_2\text{Ti}_2\text{O}_7$,” *Phys. Rev. Lett.* **109**, 077204 (2012).
 - 49 F.-Y. Li, Y.-D. Li, Y. B. Kim, L. Balents, Y. Yu, and G. Chen, “Weyl magnons in breathing pyrochlore antiferromagnets,” *Nature Communications* **7**, 12691 (2016).
 - 50 T. Moriya, “Anisotropic superexchange interaction and weak ferromagnetism,” *Phys. Rev.* **120**, 91–98 (1960).
 - 51 A. M. Cook, S. Matern, C. Hickey, A. A. Aczel, and A. Paramekanti, “Spin-orbit coupled $j_{\text{eff}} = 1/2$ iridium moments on the geometrically frustrated fcc lattice,” *Phys.*

- [Rev. B **92**, 020417 \(2015\)](#).
- ⁵² A. A. Aczel, A. M. Cook, T. J. Williams, S. Calder, A. D. Christianson, G.-X. Cao, D. Mandrus, Yong-Baek Kim, and A. Paramakanti, “Highly anisotropic exchange interactions of $j_{\text{eff}} = \frac{1}{2}$ iridium moments on the fcc lattice in La_2BIrO_6 (B=Mg,Zn),” [Phys. Rev. B **93**, 214426 \(2016\)](#).
- ⁵³ Kate A. Ross, Lucile Savary, Bruce D. Gaulin, and Leon Balents, “Quantum Excitations in Quantum Spin Ice,” [Phys. Rev. X **1**, 021002 \(2011\)](#).
- ⁵⁴ Y. Shen, Y.-D. Li, H. Wo, Y. Li, S. Shen, B. Pan, Q. Wang, H. C. Walker, P. Steffens, M. Boehm, Y. Hao, D. L. Quintero-Castro, L. W. Harriger, L. Hao, S. Meng, Q. Zhang, G. Chen, and J. Zhao, “Spinon fermi surface in a triangular lattice quantum spin liquid YbMgGaO_4 ,” arXiv preprint 1607.02615 (2016).
- ⁵⁵ J. M. Luttinger and L. Tisza, “Theory of dipole interaction in crystals,” [Phys. Rev. **70**, 954–964 \(1946\)](#).
- ⁵⁶ A. A. Soluyanov, D. Gresch, Z. Wang, Q. Wu, M. Troyer, X. Dai, and B. A. Bernevig, “Type-II Weyl semimetals,” [Nature \(London\) **527**, 495–498 \(2015\)](#).
- ⁵⁷ “Brillouin zone,” Wikipedia.